

# Mitigating Intrinsic Defects and Laser Damage using Pulsetrain-burst (>100 MHz) Ultrafast Laser Processing

Luke McKinney,<sup>a</sup> Felix Frank,<sup>a,d</sup> David Graper,<sup>a</sup> Jesse Dean,<sup>a</sup> Paul Forrester<sup>a</sup>, Maxence Rioblanc<sup>b</sup>, Marc Nantel<sup>c,a</sup> and Robin Marjoribanks<sup>a</sup>

<sup>a</sup> Department of Physics, and Institute for Optical Sciences, University of Toronto  
60 St George St., Toronto, ON M5S-1A7, Canada;

<sup>b</sup> Ecole Supérieure d'Optique  
Centre Scientifique d'Orsay, Bât. 503, 91403, ORSAY Cedex, France

<sup>c</sup> Photonics Research Ontario, OCE Inc.  
156 Front St. W, Suite 200, Toronto, ON M5J 2L6, Canada

## ABSTRACT

Ultrafast-laser micromachining has promise as an approach to trimming and 'healing' small laser-produced damage sites in laser-system optics — a common experience in state-of-the-art high-power laser systems. More-conventional approaches currently include mechanical micromachining, chemical modification, and treatment using *cw* and long-pulse lasers. Laser-optics materials of interest include fused silica, multilayer dielectric stacks for anti-reflection coatings or high-reflectivity mirrors, and inorganic crystals such as KD\*P, used for Pockels cells and frequency-doubling. We report on novel efforts using ultrafast-laser pulsetrain-burst processing (microsecond bursts at 133 MHz) to mitigate damage in fused silica, dielectric coatings, and KD\*P crystals. We have established the characteristics of pulsetrain-burst micromachining in fused silica, multilayer mirrors, and KD\*P, and determined the etch rates and morphology under different conditions of fluence-delivery. From all of these, we have begun to identify new means to optimize the laser-repair of optics defects and damage.

**Keywords:** materials processing, ultrafast laser, pulsetrain-burst, damage threshold, laser micromachining, fluence delivery, fused silica, multilayer, KDP, fluence division

## 1. INTRODUCTION

In modern high-intensity laser applications using large-diameter optics, laser damage is a common concern for the lifetime and practicality of the components.<sup>1</sup> Large optics approaching 1 meter in diameter, in particular, require a routine method of repairing and mitigating damage — such optics cannot practically be defect-free in manufacture. The main optical materials of interest include hafnia/silica multilayer dielectric stacks for mirrors and polarizers, fused silica lenses and windows, and deuterated KDP crystals (KD\*P) used for Pockels cells and frequency doubling and tripling. Defects can be categorized as: intrinsic defects that are residual from fabrication; defects created during processing and handling of the optical component; and defects created during repeated exposure to high-fluence laser irradiation. Methods are being developed to ensure that these optics can be salvaged, by minimizing the defects before installation, or mitigating laser-induced damage, so that flaws will not grow during routine laser exposure. The methods of mitigation must be effective, quickly accomplished, and meet practical standards of clean-room use. Approaches under investigation include: CO<sub>2</sub>-laser processing (melting and re-healing damage sites in fused silica); microscopically controlled chemical dissolution of material to re-form the surface (e.g., in KD\*P crystals); and mechanical micromachining of the surface at a damage site, to remove material and leave a deeper but smoother feature behind which is less susceptible to optical damage.

---

Send correspondence to: L. McKinney, E-mail: mckinney@physics.utoronto.ca, Telephone: 416 978 4400

<sup>d</sup> current address: Universität Heidelberg, Seminarstr. 2, 69117 Heidelberg

One proposal has been to use ultrafast laser machining to mitigate against original damage by cutting out localized fabrication defects in a new optic before they can cause catastrophic damage during use. For areas already laser-damaged, trimming and 'healing' small damage sites can change their damage-threshold and make them safer to use, before the damage can accumulate to a significant fraction of the area of the optic. Mitigation must create a very clean (no recast or debris) crack-free surface, as both debris and cracks lead to further damage problems. In the field of laser-processing of materials, the extension in recent years to picosecond and subpicosecond lasers has brought attention to the important differences between conventional micromachining science, using nanosecond lasers, and new strong-field interactions driven exclusively by intense ultrafast laser pulses. Shorter-duration pulses provide more precise etch-control and leave negligible residual thermal stress, features useful for application to a diverse range of materials, including transparent ones such as glass. While the technical merits of ultrafast-laser material processing have been explored in recent years,<sup>2</sup> studies of transparent materials have mainly focused on damage-threshold studies<sup>3-7</sup> and micromachining demonstrations<sup>8-10</sup> using only modest laser fluence values of  $F = 1 - 50 \text{ J cm}^{-2}$ ; there has been relatively little examination of ultrafast laser-processing at intensities well beyond threshold.

The qualitative differences observed in using different laser wavelengths, *cw* or pulsed operation, and more recently the striking differences afforded by ultrafast laser pulses over nanosecond pulses, highlight that remarkable differences arise from the manner in which specific energy is delivered to a material. Fixing a certain energy in a pulse, and delivering that energy in a nanosecond pulse implies a certain E-field strength, whereas delivering the same energy in a femtosecond-range pulse implies an enormously different E-field strength, which may carry a fundamentally different relation to the basic properties of the material. Thus, in time, the *mode of fluence-delivery* is a control-parameter that can change the characteristics of laser-micromachining, for basic reasons. At the University of Toronto, we have previously shown the possibility of using microsecond bursts of extremely high repetition rate (133 MHz) amplified picosecond laser pulses to machine clean holes in fused silica<sup>11</sup> and aluminium.<sup>12</sup> By this, we have a flexibility in fluence-delivery that lets us exploit the benefits of microsecond delivery (pulsetrain length) and the benefits of ultrafast delivery (individual pulses). We have seen that in the context of single shots we can deliver fluences of many  $\text{kJ cm}^{-2}$ , which is aggressive, while in the context of individual pulses we deliver a per-pulse fluence well below the typical single-pulse damage threshold, which is extremely gentle.<sup>13</sup> One of the characteristics of ultrafast pulsetrain-burst processing of brittle materials such as fused silica is that this approach leaves behind a low level of residual heat from one 1ps pulse to the next one, 7.5 ns later; this low level of heating makes the brittle material ductile. Consequently, we can perform ultrafast-laser materials processing on a material modified by the pulsetrain-burst, which reduces shock propagation, minimizes stresses created by thermal cycling at the laser repetition-rate, and provides a degree of control over annealing or healing damage in the material.

In this article we report using ultrahigh-repetition-rate (133 MHz) laser pulsetrain-bursts of  $0.1 - 10 \mu\text{s}$  duration, energies up to 15 mJ per shot, and individual-pulse durations of  $1 - 10 \text{ ps}$ , to process optical materials with an aim of mitigating damage subsequently caused by nanosecond high-energy laser pulses. We have characterized the morphology of machining by ultrafast pulsetrain-bursts in fused silica, dielectric coatings, and KD\*P crystals, determined the longitudinal and transverse etch rates, and identified how to control machined surface features and surface smoothness. We have also determined the effect of pulsetrain-duration on features of the ablated, annealed and reconditioned surface. From new understanding of the physical processes playing a part in this new mode of fluence-delivery, we have begun to identify new means to optimize the laser-repair of optics defects and damage.

## 2. EXPERIMENTAL SETUP

The laser used in these experiments is a flashlamp-pumped picosecond Nd:glass system ( $\lambda = 1054 \text{ nm}$ ) purpose-built at the University of Toronto.<sup>14</sup> An oscillator with active-passive and feedback-controlled modelocking produces a quasi-cw pulsetrain of over 3000 pulses, with pulse duration adjustable in the range  $1.2 - 10 \text{ ps}$  (Figure 2). At the oscillator, intrinsic pulse energies are up to  $1 \mu\text{J}$ , with interpulse separations of 7.5 ns (133 MHz). A Pockels cell *N*-pulse slicer selects a square burst of pulses from the train,  $0.05 - 10 \mu\text{s}$  long, for further amplification (Figure 1). Two multi-pass Nd:glass amplifiers increase the per pulse energy to up to  $\sim 10 \mu\text{J}/\text{pulse}$ ,

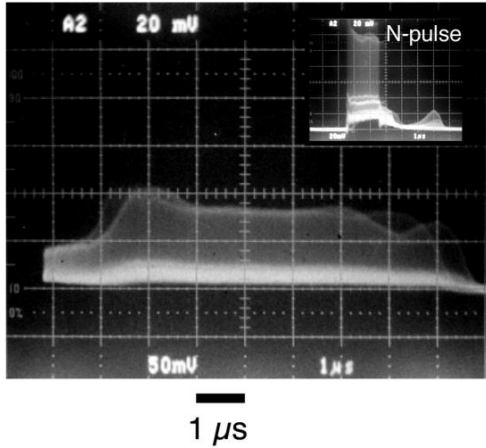


**Figure 1.** Oscilloscope trace of the pulsetrain-burst ultrafast-laser output: 10 – 3000 nearly equal-intensity pulses, 1.2 – 10 ps each, 7.5  $\mu$ s between pulses (133 MHz); up to 10  $\mu$ J/pulse, 15 mJ/pulsetrain-burst. An *N*-pulse Pockels-cell slicer controls duration of the burst (inset).

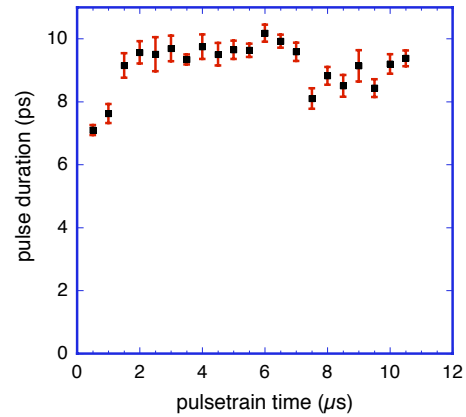


**Figure 2.** Evolution of pulse-duration within a pulsetrain-burst, as configured for these studies; measured using FROG. Laser may be configured 1.2 – 10 ps pulse-duration, adjustable pulsetrains 0.1 – 10  $\mu$ s long.

giving a total train energy of up to 12 mJ in a 10  $\mu$ s burst. The oscillator is part of a chirped pulse amplification (CPA) system, not used in this work.

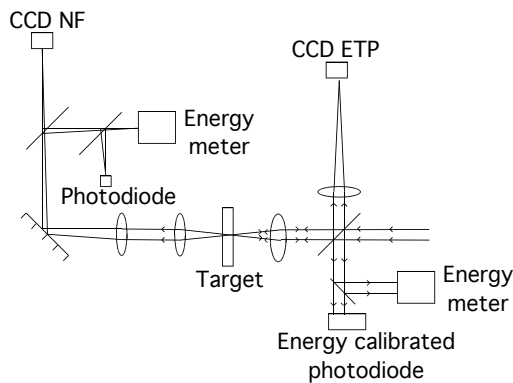


**Figure 3.** Schematic of equivalent target-plane (ETP) and near field (NF) imaging. The main benefits are likely to appear when the pulse duration is short compared to characteristic thermal or hydrodynamic timescales of materials-processing, but the pulsetrain-duration is relatively long. One aspect of these studies, therefore, is to examine the impact of pulse-duration and of pulsetrain-duration on micromachining and materials-processing.

Ultrafast laser pulses produce high fields, and optical breakdown in transparent media, while relatively modest fluences are delivered. At the same time, the brief pulse-duration means that little transport of heat into the material takes place during the pulse. One effect of this is that the volume of material heated is very shallow during the irradiation; once the pulse is over, the subsequent expansion, at a rate characteristic of the composition and temperature of the heated material, doubles the volume of the heated material much sooner than happens for a thicker layer heated by a long-pulse laser. As a result, the heated volume cools much more quickly, and

For the current studies, the beam was focussed using either 13.8mm or 30mm focal length lenses. Focal spot imaging showed elliptical focal spots of size  $5\mu\text{m} \times 7\mu\text{m}$  and  $10\mu\text{m} \times 15\mu\text{m}$ , respectively. Targets were mounted on an *xyz* translation stage of micrometer precision. Temporal profiles and total energies of the pulsetrains were measured for incident and transmitted beams. Optimal focussing was regularly monitored by autocollimating the retro-reflected beam, from which an equivalent-target-plane (ETP) image was recorded on each shot (Figure 3). A near field (NF) image of the beam waist was also captured for transparent targets. All shots were performed in air with the laser at normal incidence to the target.

### 3. PICOSECOND PULSE-TRAIN MACHINING

The mix of timescales (pulse-duration and pulsetrain-duration) involved in pulsetrain-burst processing gives new dimensions of control of the fluence delivered to the target. The main benefits

thermally decouples from the colder substrate more rapidly, than for longer laser pulses. Consequently, the thermal imprint on the material is much reduced.

Pulsetrain-burst processing affords the possibility of controlling the residual heat left in the material between pulses. Micromachining, for instance, can be modified because pulsetrain-burst processing proceeds on a material that the pulsetrain itself has modified — for instance, making brittle glass progressively more ductile during machining by a long train of pulses at near-threshold intensity, resulting in a smooth hole with no cracking (Fig. 4).

### 3.1. Fused Silica

Fused silica is a widely used optical material, chosen for its extended transparency in the UV region, and for its low levels of impurities that can cause absorption in the visible or infrared as well, lowering the damage threshold of other glasses. It also has excellent thermal, dimensional and chemical stability.

Fused silica optics damaged by high-power lasers have been successfully salvaged by microprocessing with CO<sub>2</sub> laser radiation: small laser-damage spots on this amorphous material can be melted and allowed to resolidify, eliminating cracks and restoring a surface with a distorted figure only over a small region compared to the total optic area, but much smoother on a microscopic scale and less susceptible to further laser-induced damage. Some of the same aspects are retained with long-pulsetrain-burst ultrafast-laser processing, while new possibilities in control of substrate heating, material removal, and substrate stress are afforded by picosecond and subpicosecond pulses.

#### 3.1.1. Damage mechanisms

Damage mechanisms for picosecond and femtosecond ultrafast-laser pulses in optically transparent media have been studied by a number of researchers.<sup>15–17</sup> Seed electrons are generated by tunneling ionisation, from defect states or by multi-photon absorption, and then in the laser field they rapidly generate a dense plasma by collisional avalanche-ionisation. To produce melting and vaporization, laser energy absorbed by electrons must be transferred to the material lattice by phonon emission; for very short laser pulses the timescale of this transfer may be comparable to nonlocal electron transport and expansion outward of an electron plasma (not locally quasineutral) from the very thin heated layer, which can convert electron thermal energy to secular kinetic energy. This may lead to partial decoupling of the deposited laser energy from the nominal process of thermalization into the lattice.<sup>18</sup> Perhaps more significantly, for ultrafast-laser pulses the range of thermal transport and coupling into the lattice is small on the laser timescale; the rarefaction of ionized material is at a nearly constant rate determined by material composition and temperature, and thin layers experience a proportionally greater volumetric expansion. Consequently, such thin layers cool by expansion more quickly, converting thermal energy into kinetic energy and decoupling the heated matter more quickly, reducing thermal transport into the substrate. As a result, laser micromachining by single ultrafast pulses near threshold intensities produces much less thermal damage, and begins to resemble a process of direct material sublimation.

For intense ultrafast pulses, as for longer laser pulses, the cascaded ionization process and dense plasma formation results in the formation of a critical-density surface in the plasma; laser power is absorbed in the underdense plasma, through inverse bremsstrahlung, and in the dense plasma by linear and nonlinear plasma processes. Once a dense plasma has been formed, the main process in material-removal is plasma-mediated ablation. Depending on surface geometry, plasma formed from the target persists for many nanoseconds, at the critical density, and many microseconds for low densities of underdense plasma. For repetition rates of a kilohertz and higher, subsequent pulses are incident not on bare target, but an underdense plasma. In our case, once there has been optical breakdown, the plasma formed will be pumped for the rest of the pulsetrain and

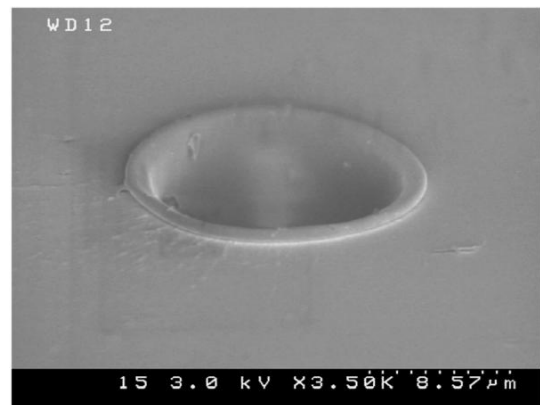


**Figure 4.** SEM image of high-aspect-ratio hole in fused silica drilled by single pulsetrain-burst: 430 pulses each of 1.2 ps duration; integrated fluence 43 kJ cm<sup>-2</sup>, etch-depth > 30 μm

so material removal proceeds by a combination of dense-plasma-mediated ablation and 'fresh' laser ablation (in conditions where the plasma becomes thin enough for sufficient energy to penetrate to the material).

At some laser wavelengths and for certain materials, 'incubation' effects are understood to play a role in laser micromachining, in which a number of nominally sub-threshold pulses accumulate subtle changes in the structure or chemistry of the material, pre-conditioning the material before ablation begins, possibly at a reduced threshold. Given the large number of pulses delivered in pulsetrain-burst processing, it was useful for us to characterise the damage thresholds, and to compare them with single-pulse thresholds. Additionally, the effect of preformed plasma seen by subsequent pulses makes it important to characterise the pulsetrain-burst etch rates in this material, which certainly should differ from that of a train of isolated single pulses.

### 3.1.2. Damage threshold for pulsetrain bursts

Single pulsetrains of individual pulsewidths  $\sim 9$  ps, varying energies, and of  $10\mu\text{s}$  duration were focussed onto polished fused silica (Corning C7980, scratch/dig 10-5) using an  $f = 13.8\text{mm}$  aspherical lens. Optical breakdown, when it happened, was noted from the sudden reduction in laser light transmitted at the surface, following plasma formation (Fig. 5). Visible-light microscopy afterwards confirmed that this was a good indication of damage in our case; these both correlated perfectly with the observation of a visible spark. From these data, for multiple shots, the damage threshold for pulsetrain-bursts was found, as shown in Figure 6.

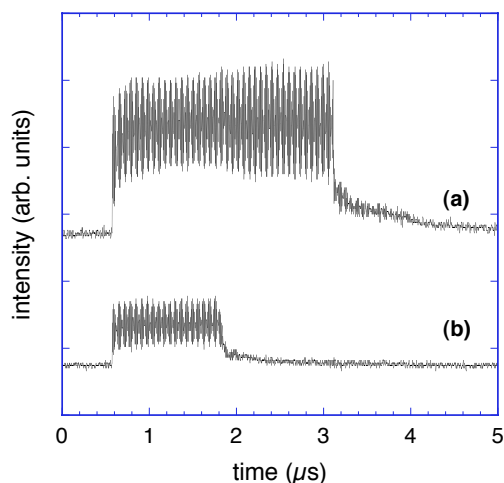


**Figure 5.** Incident (*top*) and transmitted (*bottom*) burst-pulsetrains, together, the point of optical breakdown, for near-threshold processing. The length of the pulsetrain active in micromachining, after breakdown, can be inferred. (Fine structure is digital aliasing of the pulsetrain)

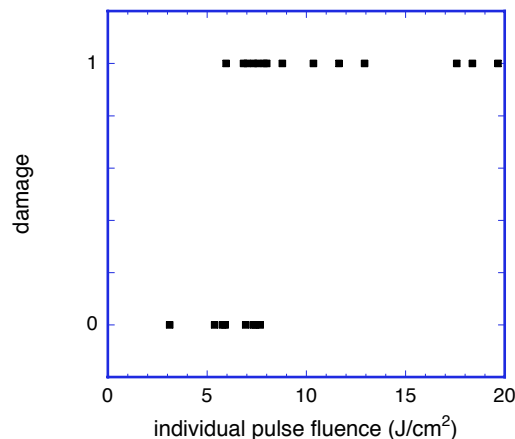


**Figure 6.** Breakdown of fused silica as a function of individual-pulse average fluence. The time-resolved data (see Fig. 5) was used to identify the individual pulse at the breakdown point within the  $10\mu\text{s}$  pulsetrain-burst.

The average fluence is calculated over the FWHM spot size. We see breakdown occurring at around  $6 \pm 1$   $\text{J}/\text{cm}^2$  per individual pulse within the train. The time-resolved data (Fig. 5) permitted identification of the particular pulse which induced breakdown — where the pulsetrain slowly grew in intensity, it was possible to determine the breakdown threshold from a single shot. Breakdown occurs during a pulsetrain when approximately this intensity is reached, or for pulsetrains above this intensity breakdown is immediate (within 25 ns). We did not observe any effect associated with the number of pulses preceding the pulse which initiated breakdown — the effect appears to be locally determined by the peak intensity, and not by effects associated with incubation.

This pulsetrain-burst value compares with a value of approximately  $4\text{ J}/\text{cm}^2$  for single 6 ps pulses from Stuart,<sup>19</sup> and  $5.5\text{ J}/\text{cm}^2$  for single 1.2 ps pulses measured previously by our group.<sup>11</sup>

### 3.1.3. Repeatability of micromachined features

Despite the various processes and parameters involved in pulsetrain-burst hole drilling (picosecond pulses, microsecond pulsetrains, long timescales for heating, repeated interaction with the breakdown plasma) the resulting machined features are found to be stable and repeatable. Nine repeated shots were made with the same parameters (pulsetrain length, focussing conditions) and having a 6% variation in energy. The resulting holes were all similar, with depth variations of 5%, and width variations of 4% — each less than the input-energy variation.

### 3.1.4. Evolution of machined hole with length of drilling pulsetrain

In order to better understand the drilling mechanisms at work we studied the evolution of the drilled-hole profile for shots of increasing pulsetrain length but constant pulsetrain-power and focussing conditions. For this purpose, we tracked the length of the active pulsetrain-burst, as measured from the onset of optical breakdown, ignoring transmitted energy before that point: we refer to this as the *drilling pulsetrain-length*. The power of the drilling train is seen to be constant over time — the time-resolved pulsetrain indicates this directly, and a plot of integrated energy versus pulsetrain length for the drilling trains is linear with a fit-parameter of  $R^2 = 0.9$ . The average power of the pulsetrain-burst was  $0.76 \pm 0.19$  kW. Profile-images of the drilled holes are given in Figure 7; from such images, the entrance-hole widths and hole-depths plotted against drilling time are shown in Figure 8.

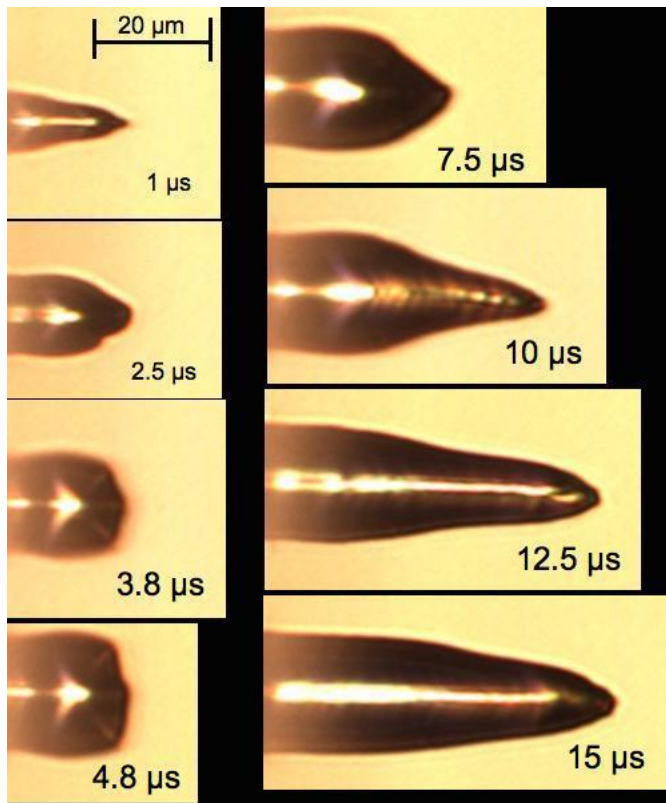


**Figure 7.** Profiles of holes drilled by increasing length of pulsetrain-bursts. Each is a single shot, drilled with the same average laser power,  $P = 0.76 \pm 0.19$  kW;  $5.7 \mu\text{J}/\text{pulse}$ .

From these images we can see that the hole, initially, is created with a nearly-constant depth and that the hole diameter grows with drilling pulsetrain-length — which hints at the ablation mechanisms involved in this ultrafast-repetition-rate machining. Additional pulses do not at first increase the depth, but rather widen the existing hole from a pointed-tipped cone to a curved barrel-like shape, with the fattest part of the cylinder wider

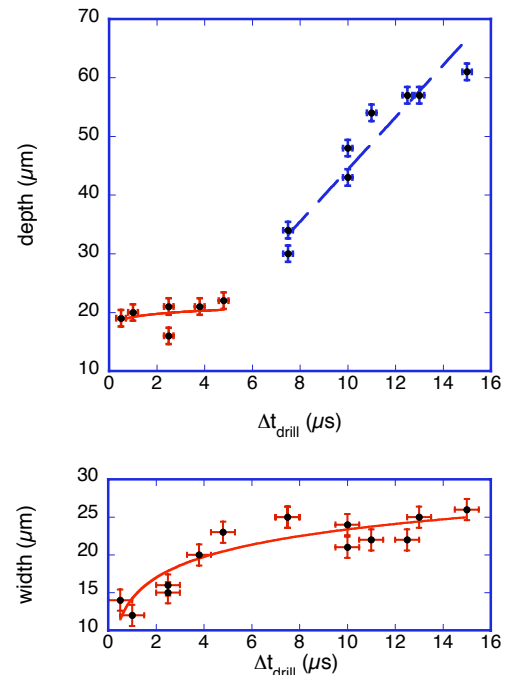


**Figure 8.** *Top:* Depth of hole *vs.* drilling-pulsetrain length; two separate trends clearly visible. *Bottom:* Entrance-hole width *vs.* drilling-pulsetrain length (same scales). Initially the hole grows in width, then width saturates and the hole grows in depth. Single shots,  $P = 0.76 \pm 0.19$  kW.

than the surface entrance-hole (left side of Fig. 7). This is the plateau noted in the depth trend in Fig. 8. Once the hole has reached a width of about  $20\ \mu\text{m}$  (an aspect ratio  $\sim 1:1$ ), drilling further into the material from the base of the cylinder recommences.

When drilling recommences (right side of Fig. 7), it extends a tapering cone down into the material, in the same shape as the first cutting, and gradually lengthens the cylindrical section. In all holes there is a small sharper tip, the most recently directly ablated region which has not been smoothed or widened by subsequent pulses. Conversely, the walls of the hole nearer to the surface appears more highly smoothed and polished. This two-stage morphology of a smooth cylinder led by a narrower tip, is uniformly present; an even clearer example of this bimodal shape — and presumably underlying bimodal drilling mechanism — is seen in a higher energy  $8\ \mu\text{s}$  pulsetrain-drilled hole in Figure 9.

This evolution in shape can be understood in terms of plasma persisting in holes between shots. When a dense plasma is generated, it effectively absorbs the incident laser energy and prevents it from reaching the surface to ablate by direct coupling (though some may still be transmitted). Further ablation is caused by plasma-mediated ablation of the material around it, expanding the hole out sideways as the plasma is fed energy (this also explains the concave shape of the hole walls). When the hole reaches a certain size, we speculate that the plasma density typically falls enough between pulses in the train for laser light to penetrate to the bottom at sufficient intensity to continue ablating directly. Other factors are possible: we have identified, in pulsetrain-burst drilling of metallic targets, that the optical physics of sending the gaussian beam into a cylindrical waveguide leads to dispersive effects which affect the transverse coherence of the beam, altering the phase and intensity within the channel, and also transforming the gaussian beam parameter.<sup>13</sup> This can significantly alter the etch rate and morphology.

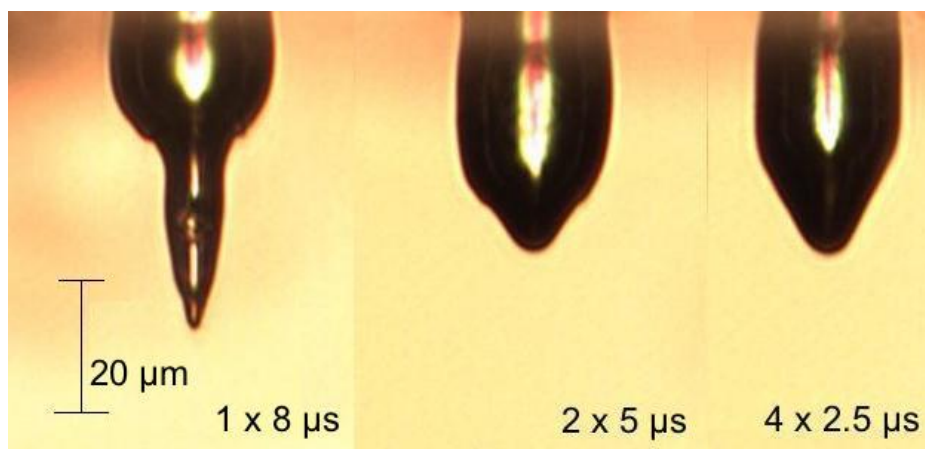


**Figure 9.** Holes resulting from (left to right): 1, 2 and 4 shots. Same integrated fluence of  $F = 26 \pm 2\text{kJcm}^{-2}$ .

### 3.1.5. Effects of fluence division

The bimodal morphology observed above suggests that in ultrafast pulsetrain-burst processing there are two stages of micromachining, suggesting two mechanisms, one of them clearly dense-plasma-mediated ablation. Measurements of damage-threshold did not suggest an incubation effect, but the plots of etch depth *vs.* effective pulsetrain length suggest an initial 'investment' in drilling that may be a consequence of dissipating preformed plasma, but which may also be a consequence of preconditioning the fused silica in advance of etching it.

To help elucidate the mechanisms of the two apparent stages, we investigated the effect of dividing a fixed integrated fluence among multiple pulse trains, *i.e.*, drilling with same total energy, but starting the process over again, multiple times (Fig. 9). An integrated fluence of  $26\ \text{kJ/cm}^2$  was delivered as 4 shots of  $2.5\ \mu\text{s}$ , 2 shots of  $5\ \mu\text{s}$ , and a single shot of  $8\ \mu\text{s}$ . The results are as may be expected, based on the upper part of Fig. 8 — the single long pulsetrain leads to the deepest hole with the most clearly visible two-stage drilling process. The multiple shorter pulsetrain holes are shorter, as expected, but also less featured — the narrow taper associated

with the first microsecond of machining is not accentuated, but the holes are more barrel-shaped. The  $2 \times 5 \mu\text{s}$  pulsetrain hole shows the beginning of bimodal structure, while in the  $4 \times 2.5 \mu\text{s}$  hole the features have been smoothed out by ablation. Rather than the multiple-shot delivery benefitting from a direct-etch interaction multiple times, they seem to have been affected by multiple contributions of plasma-mediated processing. This suggests that the first few microseconds of interaction may be taken up by establishing a steady-state plasma in a confined geometry, and that the second stage of deeper etching depends on this — thus it may be that the effect of dividing the fluence-delivery into multiple shots is simply to repeat this 'overhead' investment before deeper processing can take place. This may well prove advantageous in mitigation of damage in optics, since typically shallow processing is needed, and repeatability is an asset as the processing laser may raster-scan over the damage site.

### 3.1.6. Effect of multiple shots on one site

Another subject investigated was the effect of shooting multiple pulsetrains onto one site. From Figure 10 we can see the development of deep holes by repeated pulsetrain burst ablation. The single shot hole has a clear bimodal shape, as before. The hole evolves as we would expect from the previous results from fluence division — subsequent pulses ablate deeper into the material, smoothing out the profile of the hole into a cylinder topped by a tapering cone. The smoothing effects of subsequent ablation are clearly visible: the cylindrical base is quite smooth and feature free, while in all cases the tip (the last region to be ablated, with no following pulses) is rougher and more uneven. This basic structure is extended by following shots until a maximum is reached, after which further ablation does not occur.

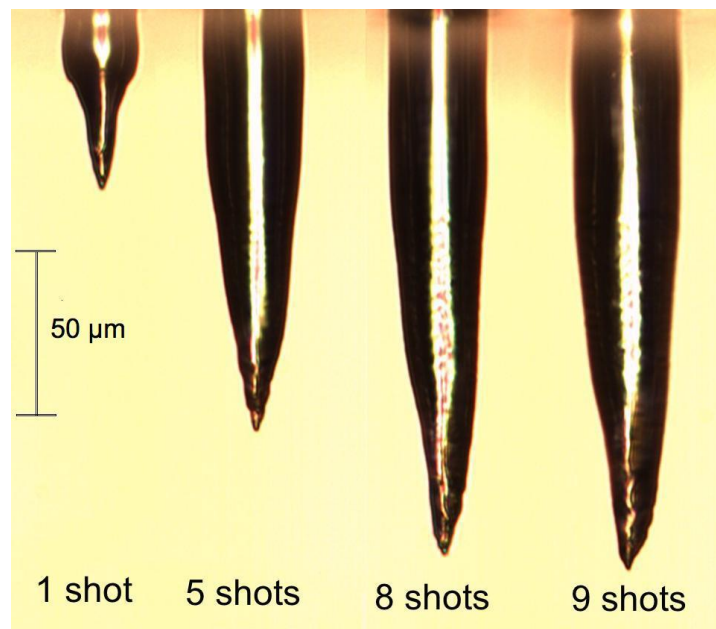


**Figure 10.** Profiles of holes drilled from top with multiple shots per site, each shot  $F = 32 \pm 0.4 \text{ kJcm}^{-2}$ . Shot-count shown includes only shots creating visible spark; right-hand image had 20 shots delivered, 9 creating apparent damage.

From hole profiles such as those shown in Figure 10, the dependence of etch-depth on number of accumulated shots was determined. As the holes became deeper, a limit was reached beyond which very rarely was there a spark evidencing damage; therefore the data are presented in two ways: etch depth *versus* number of shots delivered (Figure 11, left), and etch depth *versus* the number of those shots clearly producing damage (Figure 11, right).

As a function of shots delivered, the etch-depth is seen to saturate, limited at around  $160 \mu\text{m}$ , with an aspect ratio over 5:1. The Rayleigh range of the lens used for the smallest dimension of the focal spot is  $\sim 100 \mu\text{m}$ ; in

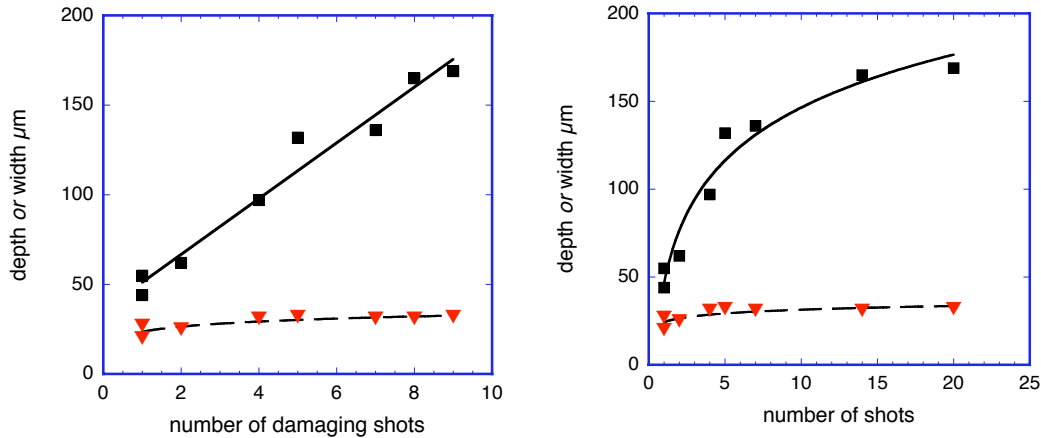


**Figure 11.** Multiple shots on fused silica: Depth (*upper, squares*) and width (*lower, triangles*) versus number of damaging shots (*left*) and total number of shots (*right*),  $10\mu\text{s}$  pulsetrains, each shot  $F = 32 \pm 0.4\text{kJcm}^{-2}$ .

that context, it seems reasonable that the beam may be partially guided within the waveguide of its own drilled channel, and that when there is optical breakdown of the smooth re-melted wall there may be additional guiding effects from plasma generated at the wall, which has a refractive index less than 1. For deep holes, and with the side-walls already enlarged to the limit of the local laser intensity, the pulse intensity may fluctuate slightly around the threshold for optical breakdown, but soon have found its limit and saturate.

With the same data plotted against the count of shots that produce damage, according to visible sparking, we can see that the depth increases linearly with the number of shots: where there is sufficient intensity to reach optical breakdown, and create linear absorption, there is sufficient energy in the rest of the train to etch further — a situation different from ultrafast micromachining at lower repetition-rates. In this sense, the etch-depth is limited by the critical value for optical breakdown, and the optical physics of ultrafast pulse propagation, group-velocity dispersion and interference in the waveguide structure is of key importance.

In reflecting the underlying mechanisms of laser-etching using pulsetrain-bursts, it's significant to note that the etch-depth versus number of damaging shots does not pass through zero. This is interpreted as the first shot drilling more effectively than the others, perhaps because of easier dissipation of plasma, or because of optical effects of propagation at the glass surface, while subsequent pulses are directed into a hole and must dissipate plasma from the channel, as well as no longer etching at the focal plane. The width reaches a maximum after 4 shots and does not increase, though we note that the surface around the hole can be affected heavily by further shots, as shown in Figure 12.

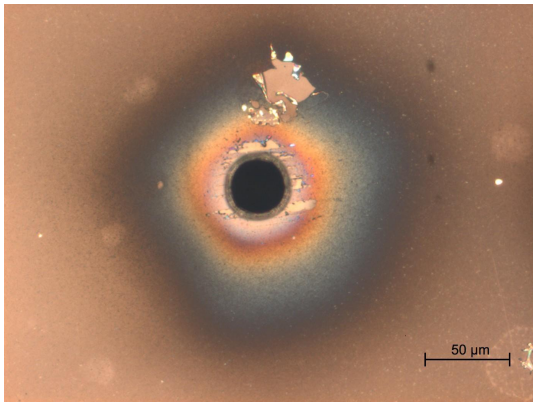


**Figure 12.** Surface view of fused silica etched with 20 shots in total, nine absorbed (total  $F = 272\text{kJcm}^{-2}$ ). Heavy recoating by fused silica plume, redeposited in air, produces interference rings. *top*: layer peels cleanly from the surface.

### 3.2. Dielectric Mirrors

Damage of multilayer dielectric stacks, used for mirrors and for polarizers, by high-power lasers is typically of four major types: delamination of the deposited layers; flat-bottomed pits etched through the coatings; material scalding by hot plasma evolved from damage site; and pits from ejection of nodules created as flaws in the dielectric-layer deposition process.<sup>20</sup> Mitigation can be achieved in several forms: optical conditioning of defects such

as nodules, in which an optic is repeatedly laser-irradiated, starting at low fluences and increasing until any nodules are ejected at the lowest-possible energy, rather than catastrophically; delaminations may be trimmed, and sharp features that would produce field concentrations can be removed, improving the damage threshold subsequently; and attached debris, other rough features and substrate damage may be remelted and smoothed, similarly helping to proof the site against being a nucleating centre for accumulating further damage.

The dielectric mirrors used in this work were broadband  $\text{MgF}_2/\text{silica}$  dielectric mirrors, one reflective in the  $1200 - 1600\mu\text{m}$  range (Thorlabs BB1-E04), not resonant to our laser, the other high reflectance for green at  $524/532\text{ nm}$  (Thorlabs NB1-H12), resonant to a laser harmonic. These dielectric coatings were assessed for intrinsic damage threshold under irradiation by pulsetrain-bursts, and ablation morphologies and etch rates were characterised. Studies have been begun to evaluate the new damage threshold of sites that have been treated by pulsetrain-burst processing under different conditions.

### 3.2.1. Damage threshold

For dielectric stacks, deep processing is not expected to be needed. A series of  $0.5\ \mu\text{s}$  pulsetrains at integrated fluences  $0.5 - 2.5\ \text{J cm}^{-2}$  were delivered to the surface using an  $f = 30\text{mm}$  lens to find the breakdown threshold of the dielectric mirror. The laser intensity at optical breakdown was found, as before, from the time-resolved, energy-calibrated incident pulsetrain, and the integrated fluence was found by integrating the power over the drilling pulsetrain. The results are shown in Figure 13. As for the fused silica, we can see that there is a clearly defined breakdown threshold at  $0.5 - 2.5\ \text{J cm}^{-2}$ . A few shots above this intensity failed to cause breakdown, possibly due to isolated issues in focussing.

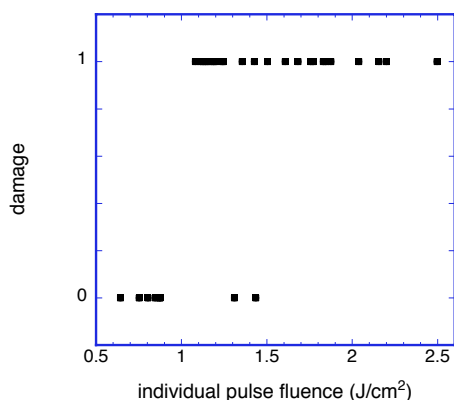


**Figure 13.** Threshold: breakdown *vs.* fluence-per-pulse for a  $15\mu\text{m} \times 10\mu\text{m}$  focal spot  $0.5\ \mu\text{s}$  pulsetrain-burst (66 pulses) incident on a broadband  $1280 - 1600\text{nm}$  dielectric mirror.



**Figure 14.**  $10\ \mu\text{s}$  laser pulsetrain at threshold fluence, on broadband  $1280 - 1600\text{nm}$  HR mirror. Clean removal of dielectric layers, some material modification on perimeter of site, and slight thermal-shock fracturing due to long-time post-train leakage. Image has been both top-illuminated and also viewed through a single polarizer.

These results were calculated from the FWHM elliptical spot size taken from calibrated images of the beam waist produced by the lens used. Breakdown occurs at a per-pulse fluence of about  $1 \pm 0.1\ \text{J}/\text{cm}^2$ .

### 3.2.2. Damage mechanisms

The multilayer coatings were irradiated with pulsetrain-bursts of length  $0.5 - 10\ \mu\text{s}$ , and with integrated fluences  $30\ \text{J cm}^{-2} - 10\ \text{kJ cm}^{-2}$ . At threshold intensities and for short pulsetrain-bursts, fine control is possible, and just a few layers may be etched (Fig. 14). Figure 15 shows the cleanly cut dielectric multilayers produced at threshold fluences in the wings of a  $26\mu\text{m}$  gaussian focal spot, which appear clearly in SEM images.

At higher fluences and longer pulsetrain bursts, a summary in images of the effect is given in Figure 16. We conclude that the length of the pulsetrain is the most important factor in determining the lateral extent of the affected region. The longest pulsetrain causes the most severe damage, not only penetrating through to the fused-silica substrate but drilling a hole in it. We see that the shorter pulsetrains both penetrate the dielectric

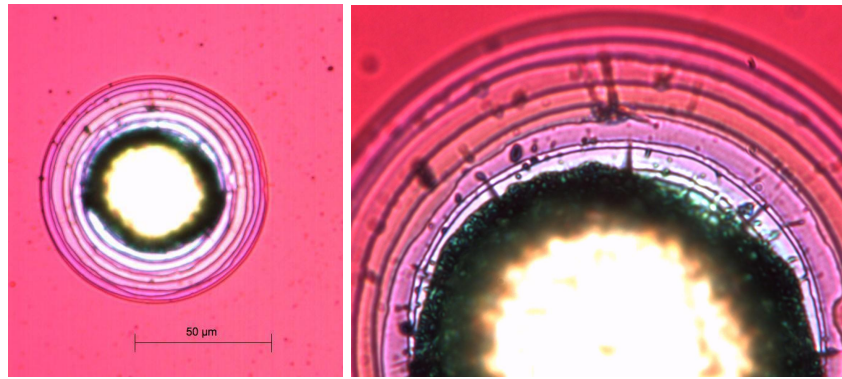


**Figure 15.** Ring structure formed on dielectric mirror by  $0.5 \mu\text{s}$  pulsetrain focussed to a  $10 \times 15 \mu\text{m}$  spot.

layer to reach the substrate and produce damaged regions of about the same size, but the lower-intensity pulse does not produce nearly as much debris, since much of the debris results from ablation of the substrate.

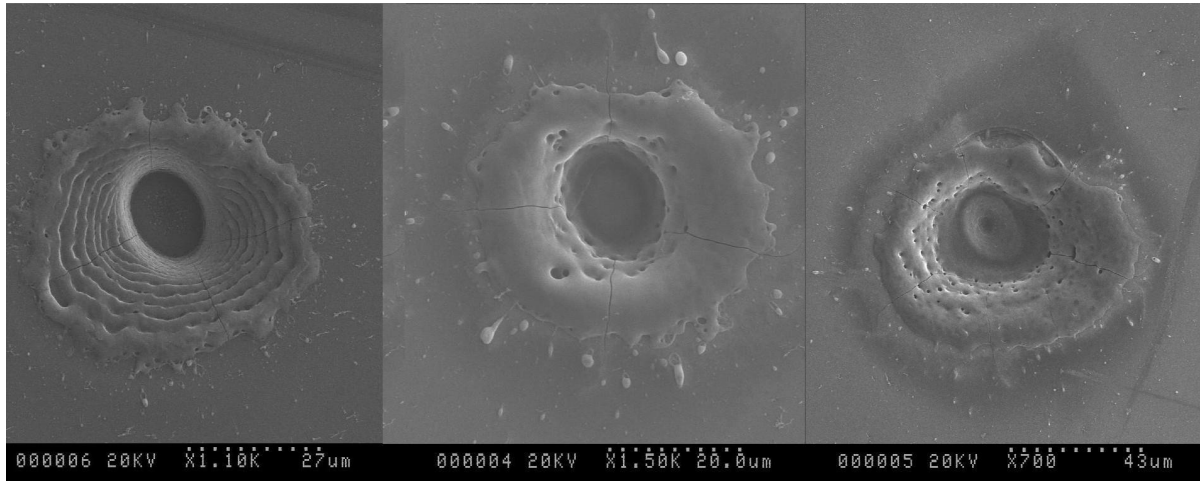


**Figure 16.** SEM images of three holes drilled in multilayer mirror. Left:  $5 \mu\text{s}$  pulsetrain at  $\sim 1.25\times$  threshold intensity, clear remelted layer structure, slight debris and some cracking on cooling. Middle:  $1.25 \mu\text{s}$  pulsetrain at  $\sim 1.25\times$  threshold intensity, plus low-level post-train leakage; displays gross melting, debris, contraction cracking. Right:  $10 \mu\text{s}$  pulsetrain, at  $\sim 5\times$  threshold intensity, plasma scalding and scarred/remelted hole walls, showing pitting and debris. Note differing magnifications.

Using short pulsetrains, we examine the damage to the multilayers more closely. Evidence that the layered structure of the dielectric has a strong effect is shown in Fig. 17 below. Here definite steps can be seen, as each successive layer is ablated more deeply. Further, each layer has a clear lip and well-defined edge — each layer is apparently ablated in sequence, rather than in bulk, with a smaller hole drilled in each subsequent layer until the substrate is reached. It appears that the thin dielectric layers are susceptible to the strain of thermal contraction after processing. Radial cracks can be seen through the melted lip and down through the successive layers (Fig. 17, left image, 12 o'clock position). These cracks result from thermal cooling after ablation has taken place, as the material cools and contracts, concentrating strains around the new hole, where material no longer participates. Concentric surface cracks observable just outside the melted rim (Fig. 17, right image) appear to be due to shock stresses from laser impact or heating early in the process, perhaps as the first effect of the laser before ablation takes place; there is evidence of partial healing or overcoating by melted multilayer material.

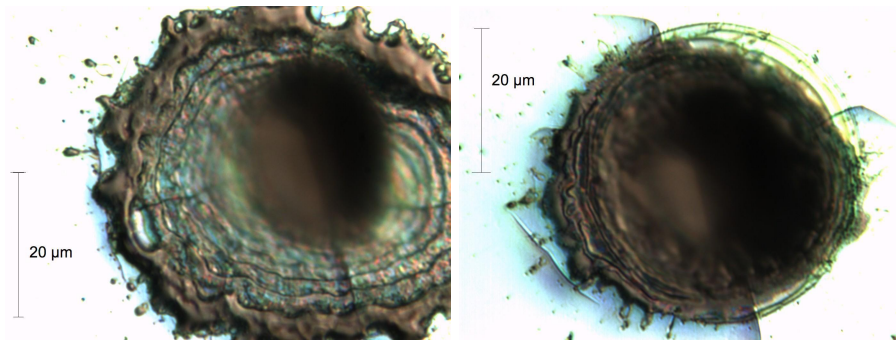


**Figure 17.** Left:  $5 \mu\text{s}$  laser pulsetrain focussed by 25 mm lens. Multilayers remain evident after etching and remelting; some cracking and irregularity evident. Right: Hole drilled with 25 mm lens and  $2.5 \mu\text{s}$  pulsetrain, exhibiting rippling on the remelted surface, intact multilayer steppes, and concentric and radial cracking. Details inside hole not visible due to limited depth-of-field.

### 3.3. KD\*P

Several methods of damage-mitigation for KD\*P are available, though none are entirely satisfactory. Dissolution of the crystal with water can refigure the surface and remove damage sites, but the process leads to recrystallization, and leaves crystallites at the site. Laser machining with ultrashort-pulsed lasers has been seen to cause excessive cracking, as does processing with  $\text{CO}_2$  lasers. Micromachining using diamond-tipped micro-routers produces clean features that improve the post-treatment damage thresholds, but problems remain with automation of the process and with debris generation and in the necessary clean-room environment

In processing with ultrafast pulsetrain-bursts, KD\*P was seen to have a much lower damage threshold than fused silica, as is the case for other intense-laser interaction. Figure 18 summarizes results graphically: there is little sign of cracking, relatively small amounts of distributed debris, and the machining done is regular and repeatable. In addition to a laser-etched central hole, there is a small ( $\sim 30 - 75 \mu\text{m}$ ) zone around the central site in which the KD\*P crystal appears to have been partially melted and recrystallized. It does not appear to be a heat-affected zone in the sense of lateral thermal transport; the dimensions of this zone are comparable to the zone of gentle processing seen around dielectric laser-etch holes, as shown in Fig. 15, and appear to be related to the low-intensity wings of the laser focal spot. In the case of KD\*P and the multilayer coatings, the observed laser-spark likely indicates the gross ablation of the central hole, but more subtle material removal likely occurs at lower thresholds. Further studies will examine this.

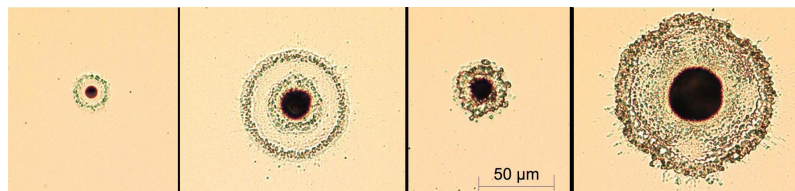


**Figure 18.** KD\*P, left to right:  $1 \mu\text{s}$  pulsetrain, just near damage threshold ( $F = 5 \text{ kJ cm}^{-2}$ ); same, four times as much energy ( $F = 22 \text{ kJ cm}^{-2}$ );  $7 \mu\text{s}$  pulsetrain, slightly above damage threshold ( $F = 16 \text{ kJ cm}^{-2}$ ); same, four times as much energy ( $F = 63 \text{ kJ cm}^{-2}$ )

Two series of shots of varying intensity were performed, with pulsetrain burst lengths of  $1 \mu\text{s}$  and  $7 \mu\text{s}$ . The results are shown in Figure 19. It can be seen that for both pulsetrains the size of the drilled hole and the larger surrounding halo zone increase in exact proportion to one another, increasing with incident intensity to a limiting value.

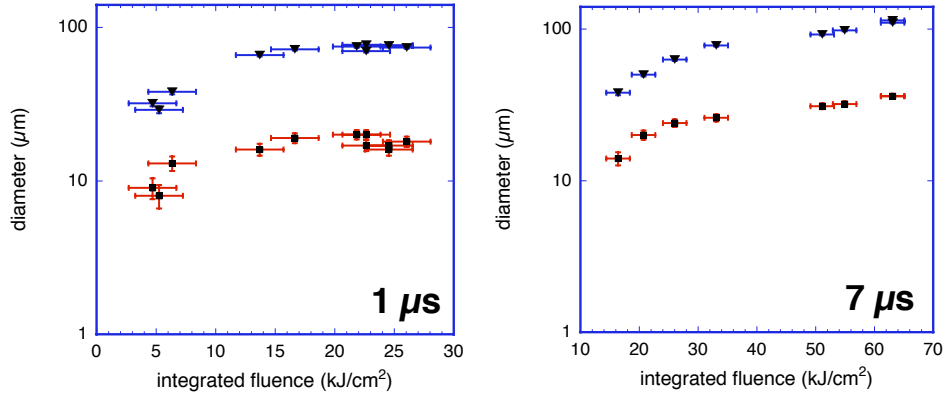


**Figure 19.** KD\*P hole-width (*upper, squares*) and halo-zone diameters (*lower, triangles*) as a function of pulsetrain fluence, for 1  $\mu\text{s}$  (*left*) and 7  $\mu\text{s}$  (*right*) pulsetrains. The halo seems to be due to energy in the focal-spot wings, and ranges in diameter from 30 – 120  $\mu\text{m}$ . Halo and crater sizes are strictly proportional. Fluences  $\pm 15\%$  systematic error.

### 3.3.1. Damage mechanisms

Damage mechanisms in KD\*P appear to be similar to those in dielectric multilayers, and in all the drilled holes we see both a clearly defined drilled hole and a small halo zone, which exactly tracks the size of the drilled hole; it does not appear to result from lateral heat transport. Both show only a slight increase in size with a sevenfold increase in pulsetrain length. Possibly there exists for pulsetrain-burst processing a threshold for material modification, below that for ablation, in which the crystalline KD\*P is melted or recast. This is in contrast to the results for fused silica. Future studies will look into the effect of different focal-spot intensity profiles.

Side-view profiles of the pulsetrain-burst drilled holes were not available; whether or not the same bimodal etching process takes place here as for fused silica will be important information from future experiments. The absence of shock-damage or thermal cracking is promising, for this approach to damage mitigation in KD\*P; we plan to evaluate the nanosecond-pulse laser-damage threshold of the central crater and the halo zone.

## 4. CONCLUSIONS

We have conducted studies of the interaction physics and basic characteristics of ultrafast pulsetrain-burst materials processing, foundational to its use in mitigating damage caused to large or difficult-to-replace optics in high-power laser systems. We have characterized the morphology of machining by ultrafast pulsetrain-bursts in fused silica, dielectric coatings, and KD\*P crystals, and found that fused silica, at least, shows that laser etching proceeds in a two-step process, involving optical breakdown of material at the extreme end of the channel, and plasma-mediated ablation, remelting, and smoothing of the channel nearer to the entrance hole. Fused silica is very successfully micromachined, and produces highly controllable and repeatable features, with very little cracking or shock damage. We conclude that some of these advantages accrue because pulsetrains of multi- $\mu\text{J}$  pulses, at multi-MHz repetition rates, leave in the material between pulses a heat sufficient to change the material characteristics, making the brittle glass more ductile. Longitudinal and transverse etch rates were established under different processing conditions, and we identified how to control machined surface features and surface smoothness. We have also determined the effect of pulsetrain-duration on features of the ablated, annealed and reconditioned surface. As with deep-etching of other materials in air, there may be redeposition of material back onto the surface; for most damage-mitigation applications we expect relatively shallow etching, and anticipate this redeposition will be at levels that will not alter the nanosecond-laser damage thresholds.

Initial results of pulsetrain-burst processing of multilayer dielectric coatings suggest that the residual heat left by pulsetrains may leave too much stress on the coatings, after processing, leading to radial cracking. We also saw indications that there is an extremely gentle regime of pulsetrain-burst processing in which layers may

be stripped cleanly and without delamination, and without cracking; this will be investigated in future, as will the effect of different focussed intensity distributions. It would be extremely interesting to apply pulsetrain-burst processing to the goal of optical conditioning, as the control parameters may be ideally suited to extremely gentle nodule removal.

Studies of processing KD\*P were preliminary but promising — ultrafast-laser processing was possible without cracking the material by thermal cycling stresses or by laser-produced shocks. Etching was well-controlled and very repeatable. Surface-modification surrounding the focal-spot centre was seen, which we attribute to low-fluence heating, over long timescales, in the wings of the focal spot; different focal-spot distributions will be investigated in future experiments.

For all these materials, the new damage thresholds under nanosecond high-power laser irradiation of sites micromachined by pulsetrain bursts will be evaluated. Future experiments will study the interaction of this processing technique with the classes of damage-feature seen in practical high power laser applications.

In summary, from new understanding of the physical processes which come into play in this qualitatively different mode of fluence-delivery, we have begun to identify new means to optimize the laser-repair of optics defects and damage.

## 5. ACKNOWLEDGEMENTS

The authors acknowledge support from the Canadian Institute for Photonic Innovations, Photonics Research Ontario, and the Natural Sciences and Engineering Research Council of Canada.

## REFERENCES

1. H. Bercegol, P. Bouchot, L. Lamaignère, B. L. Garrec, and G. Razé *Proc. SPIE* **5273**, pp. 312–324, 2004.
2. see for example in *Commercial and Biomedical Applications of Ultrafast Lasers II*, *Proc. SPIE* **3934**, 2000.
3. B. T. Vu, O. L. Landen, and A. Szoke *Phys. Rev.* **E47**, p. 2768, 1993.
4. B. T. Vu, O. L. Landen, and A. Szoke *Phys. Plasmas* **2**, p. 476, 1995.
5. D. Du, X. Liu, G. K. J. Squier, and G. Mourou *Appl. Phys. Lett.* **64**, p. 3071, 1994.
6. B. C. Stuart, M. D. Feit, and S. Herman *J. Opt. Soc. Am.* **B13**, p. 459, 1996.
7. D. von der Linde et al *J. Opt. Soc. Am.* **B13**, p. 216, 1996.
8. J. Kruger and W. Kautek *Appl. Surf. Sci.* **96-98**, p. 430, 1996.
9. H. Varel, D. Ashkenasi, A. Rosenfeld, M. Wähmer, and E. E. B. Campbell *Appl Phys* **A65**, p. 367, 1997.
10. P. R. Herman, A. Oetl, K. Chen, and R. Marjoribanks *Proc. SPIE* **3616**, p. 148, 1999.
11. P. R. Hermann, A. Oetl, K. P. Chen, and R. S. Marjoribanks in *Commercial and Biomedical Applications of Ultrafast Lasers*, *Proc. SPIE* **3616**, pp. 148–155, 1999.
12. M. Lapczynya, K. Chen, P. R. Herman, H. W. Tan, and R. S. Marjoribanks *Appl. Phys.* **A69 (Suppl)**, pp. S883–886, 1999.
13. R. S. Marjoribanks, Y. Kerachian, P. R. Herman, S. Camacho-Lopez, and M. Nantel in *Technical Digest, Conference on Lasers and Electro-Optics (CLEO), 2001 (Optical Society of America, Baltimore, MD, USA)*, *TOPS* **56**, 2001.
14. R. S. Marjoribanks, F. W. Budnik, G. K. L. Zhao, M. Stanier, and J. Mihaychuk *Optics Letters* **18**, p. 361, 1993.
15. C. B. Schaffer, A. Brodeur, and E. Mazur *Meas. Sci. Tech.* **12**, p. 1784, 2001.
16. M. D. Perry, B. C. Stuart, P. S. Banks, M. D. Feit, V. Yanovsky, and A. M. Rubenchik *J. Appl Phys.* **85**, pp. 6803–6810, 1999.
17. P. P. Pronko, P. A. VanRompay, C. Horvath, F. Loesel, T. Juhasz, X. Liu, and G. Mourou *Phys. Rev. B* **58**, pp. 2387–90, 1998.
18. P. B. Corkum, F. Brunel, N. K. Sherman, and T. Srinivasan-Rao *Phys. Rev. Lett.* **61**, pp. 2886–9, 1988.
19. B. C. Stuart, M. D. Feit, A. M. Rubenchik, B. W. Shore, and M. D. Perry *Phys. Rev. Lett.* **74**, p. 2248, 1995.
20. F. Génin and C. J. Stolz in *Third International Workshop on Laser Beam and Optics Characterization*, *Proc. SPIE* **2870**, pp. 439–448, 1996.